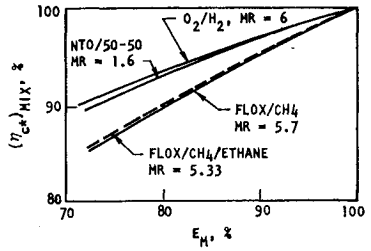

Fig. 6 Comparison of mixing limited C^* performance as a function of mixing uniformity for several propellant combinations.

relationship for E_m and mixing-limited c^* efficiency defined, then, for any desired propellant combination, the E_m required to obtain a specified c^* efficiency can be analytically determined.

We must define the allowable range in MR. The major portion of the spray from typical injectors lies in the range $0.1 \leq MR \leq 100$. Utilizing this result, the relationship between variables of Eq. (6) can be determined. This has been done for NTO/50-50 in Fig. 4. The band represents all possible solutions for $(\eta_{c^*})_{mix}$ and E_m lying between $MR = 0.1$ and $MR = 100$ for a constant overall MR of 1.6. The dashed line represents the average or mean line through the band. It is obvious from this plot that no unique or even narrow band of possible solutions exist between E_m and $(\eta_{c^*})_{mix}$ for the selected range in MR, but increasing the number of stream tubes and restricting the solutions to correspond to distributions from specific injectors considerably narrows this band.

Experimental data were utilized to determine if sprays produced by injectors would result in distributions in a narrow band around the mean line determined from the two-tube model. The mean lines for MR's of 1.0 and 2.0 utilizing NTO/50-50 propellants are superimposed on actual measured spray distribution data in Fig. 5, obtained utilizing several impinging stream injectors. Note that, over the range of E_m from about 50 to 95%, the data fall very close ($\pm 1.5\%$) to the analytically determined mean value line. Identical results have also been obtained for FLOX/CH_4/ethane propellants at $MR = 5.33$. These results also are presented in Fig. 5. Note that the data agree to within $\pm 1.0\%$ with the analytically determined mean line. Due to the excellent agreement found, the curves of the type shown in Fig. 5 can now be used to determine the influence of spray quality on performance for differing propellant combi nations.

Comparison for Several Propellant Combinations

The model just described was used to generate predictions of E_m effects on $(\eta_{c^*})_{mix}$ for four propellant combinations giving the mean line results plotted in Fig. 6. Note that O_2/H_2 is least affected by nonuniformities in mixing, while the FLOX/CH_4 plus ethane propellant are most sensitive. The NTO/50-50 propellant combination is close to the O_2/H_2 curve. The deviations in η_{c^*} for a given E_m is due to the shape of the c^* vs MR curve for each propellant.

Conclusions

A rather simple relationship between mixing uniformity E_m and mixing-limited c^* efficiency $(\eta_{c^*})_{mix}$ can be used to predict actual c^* mixing-limited performance. This relationship allows a prediction of the sensitivity to mixing of any propellant combination on η_{c^*} to be analytically determined.

References

[1] Rupe, J. H., "The Liquid Phase Mixing of a Pair of Impinging Streams," Progress Rept. 20-195, Aug. 1953, Jet Propulsion Lab., Pasadena, Calif.

[2] Rupe, J. H., "A Correlation Between the Dynamic Properties of a Pair of Impinging Streams and the Uniformity of Mixture Ratio Distribution in the Resulting Spray," Progress Rept. 20-209, March 1956, Jet Propulsion Lab., Pasadena, Calif.

[3] Rupe, J. H., "An Experimental Correlation of the Non-reactive Properties of Injection Schemes and Combustion Effects in a Liquid-Propellant Rocket Engine," TR 32-255, July 1965, Jet Propulsion Lab., Pasadena, Calif.

[4] Elverum, G. W. and Morey, T., "Criteria for Optimum Mixture Ratio Distribution Using Several Types of Impinging-Stream Injector Elements," Memo 30-5, Feb. 1959, Jet Propulsion Lab., Pasadena, Calif.

[5] Pieper, J. L., Dean, L. E., and Valentine, R. S., "Mixture Ratio Distribution—Its Impact on Rocket Thrust Chamber Performance," *Journal of Spacecraft and Rockets*, Vol. 4, No. 6, June 1967, pp. 786–789.

[6] Riebling, R. W., "Effect of Orifice Length-to-Diameter Ratio on Mixing in the Spray from a Pair of Unlike Impinging Jets," *Journal of Spacecraft and Rockets*, Vol. 7, No. 7, July 1970, pp. 894–896.

[7] Nurick, W. H. and Clapp, S. D., "An Experimental Technique for Measurement of Injector Spray Mixing," *Journal of Spacecraft and Rockets*, Vol. 6, No. 11, Nov. 1969, pp. 1312–1315.

[8] Wrobel, J. R., "Some Effects of Gas Stratification upon Choked Nozzle Flows," AIAA Paper 64-266, Washington, D.C., 1964.

Conical Nozzle Flow in the Rarefied Regime

G. T. Patterson* and M. W. Milligan†
University of Tennessee, Knoxsville, Tenn.

Nomenclature

A	=	cross-sectional area
h,h_t	=	enthalpy and total enthalpy, respectively
k	=	coefficient of thermal conductivity
L	=	length of nozzle
$\dot{m},\bar{m}$	=	mass flow rate and dimensionless values
$\dot{N},\bar{N}$	=	molecular flow rate and dimensionless value [Eq. (19)]
N	=	number of points in grid station
K_n,K_n'	=	Knudsen number and function of K_n, respectively
P_r,P_e	=	Prandtl and Reynolds numbers
p	=	pressure
q	=	heat flux
R_g	=	gas constant
r	=	radius coordinate in spherical coordinates, Fig. 1
T,t	=	temperature and time, respectively
u,u_s	=	dimensionless velocity and slip velocity, respectively
v	=	velocity when subscripted, otherwise dimensionless
$\bar{V}$	=	mean molecular velocity
z	=	nozzle longitudinal coordinate
β	=	integral limit, [Eq. (18)]
γ	=	ratio of specific heats
η,λ	=	molecular density and mean free path, respectively
θ	=	angle coordinate
θ_m	=	nozzle half angle
μ,ρ	=	viscosity and density, respectively
τ	=	shear stress
ϕ	=	angle coordinate

Subscripts

e,i	=	nozzle exit and entrance, respectively
m,n	=	grid coordinate integers

Received December 16, 1970; revision received February 5, 1971.

* Graduate Student, Mechanical and Aerospace Engineering; now First Lieutenant, Ordnance Corps, United States Army.

† Professor of Mechanical and Aerospace Engineering. Member AIAA.

0 = stagnation property
r,θ,ϕ = direction of vectors

Introduction

SPACECRAFT and various industrial processes involve high vacuum flows and require rarefied flow solutions. This Note is concerned with the flow of a perfect monatomic gas in a converging nozzle with consideration given to the near-continuum, transition, and near-free-molecular regimes. The continuum analysis includes the effect of slip velocity at the nozzle wall, and the solution is obtained by use of finite-difference methods. The diffusion analysis includes the effects of intermolecular collisions. The diffusion flow component is obtained by summing the number of molecules which cross the nozzle exit plane.

Rarefied flow has been studied for constant-area passages.[1,2] Sparrow and Johnson[3] investigated free molecular flow in a conical nozzle by analogy to radiant heat transfer. Milligan[4] formulated a finite-difference approximation to flow in a converging nozzle but was unable to obtain extensive results due to limitations in computer facilities. Williams[5] obtained a similar solution for flow in a converging nozzle with velocity slip and temperature jump. Rae[6] treated slightly rarefied flow in a converging-diverging nozzle using a finite-difference method.

Continuum Equations

The basic conservation equations (mass, momentum, and energy) are valid for all three regimes. However, before they can be solved, something must be assumed about the representation for the stresses and the heat flux. The traditionally used assumptions are Stokes' law of friction and Fourier's law of heat transfer. Substituting these relationships into the conservation equations gives the Navier-Stokes (N-S) equations.

The problem is cast in spherical coordinates. The flow is assumed to be axisymmetric and steady, and the nozzle wall angle is assumed small. With these assumptions and those of a perfect gas, the N-S equations for conservation of momentum and energy, together with the equation expressing the continuity of mass

$$(1/r^2)(\partial/\partial r)(\rho r^2 v_r) + (1/r\theta)(\partial/\partial\theta)(\rho\theta v_\theta) = 0 \quad (1)$$

and the equation of state

$$p = \rho RgT \quad (2)$$

are sufficient to describe the flowfield in the nozzle.

Solution of the full N-S equations would be a formidable task. However, an order-of-magnitude analysis may indicate some terms that can be eliminated. We considered channels that are slender, $r\theta_m/L \ll 1$ and nondimensionalized ρ, p, and v_r with respect to mean centerline values, r with respect to L, θ with respect to θ_m, and h with respect to $\bar{v}_r{}^2$. Substitution of these new variables into Eq. (1) will indicate that v_θ should be nondimensionalized with respect to $\theta_m\bar{v}_r$. At low ρ the viscous forces may become the same order of magnitude as the inertial forces. Equating these forces will indicate that μ should be nondimensionalized with respect to $\bar{\rho}\bar{v}_r\bar{r}^2/L$.

Substituting the nondimensional variables, the momentum and energy equations become

$$(1/r)\,(\partial P/\partial\theta) = 0 \quad (3a)$$

$$\rho\left(v_r\frac{\partial v_r}{\partial r} + \frac{v_\theta}{r}\frac{\partial v_r}{\partial\theta}\right) = -\frac{\partial p}{\partial r} + \frac{\mu}{r^2\theta}\frac{\partial v_r}{\partial\theta} + \frac{1}{r^2}\frac{\partial}{\partial\theta}\left(\mu\frac{\partial v_r}{\partial\theta}\right) \quad (3b)$$

$$\rho\left(v_r\frac{\partial h}{\partial r} + \frac{v_\theta}{r}\frac{\partial h}{\partial\theta}\right) = v_r\frac{\partial p}{\partial r} + \frac{1}{r^2\theta}\frac{\partial}{\partial\theta}\left(\frac{\mu\theta}{P_r}\frac{\partial h}{\partial\theta}\right) + \mu\left(\frac{1}{r}\frac{\partial v_r}{\partial\theta}\right)^2 \quad (4)$$

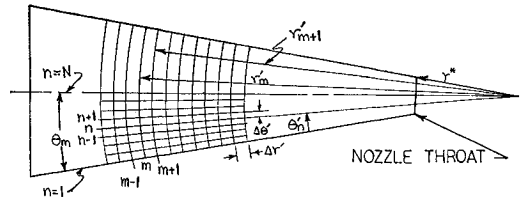

Fig. 1 Finite-difference grid.

after returning to dimensional variables. These equations are in a form similar to the slender channel equations.[7] From the order-of-magnitude analysis it was determined that p is a function of r only. To find a relationship for this observation, consider the surface integral for the mass flux through a surface of constant radius. The v_θ component of velocity will not enter into integration since it is tangent to the surface. Thus, $\dot{m} = \int_A \rho v_r dA$. Substituting the small angle expression for dA and using the perfect gas equation, we obtain

$$p = \dot{m}\Big/\left(2\pi r^2\frac{\gamma}{\gamma-1}\int_0^{\theta_m}\frac{v_r}{h}\,\theta d\theta\right) \quad (5)$$

Near-Continuum Solution

The continuum solution is extended to low Reynolds numbers, by applying slip boundary conditions. At low R_e the viscous forces will become comparable to the inertial forces. It may be assumed, then, that the flow is fully viscous. Thus, Eqs. (1–5) must be solved across the entire nozzle cross section.

Equations (3) and (4) will be placed in finite-difference form for the solution of the v_r and h profiles. The variables will be nondimensionalized as follows: $\rho' = \rho/\rho_0$, $p' = p/p_0$, $r' = r/r^*$, $\theta' = 1 - \theta/\theta_m$, $u = 2v_r/(h_0)^{1/2}$, $v = -2v_\theta/\theta_m(h_0)^{1/2}$, $h' = h/h_0$, and $\mu' = \mu/\mu_0$. For our thermally perfect gas, $\mu' = (h')^{1/2}$. Substitution of these variables into Eqs. (3) and (4), expanding the partial derivatives, and assuming P_r to be constant gives

$$\rho' u\frac{\partial u}{\partial r'} + \rho'\frac{v}{r'}\frac{\partial u}{\partial\theta'} = -\frac{4(\gamma-1)}{\gamma}\frac{\partial p'}{\partial r'} + \frac{1}{R_e\theta_m}\left[\frac{1}{2r'(h')^{1/2}}\frac{\partial h'}{\partial\theta'}\left(\frac{1}{r'}\frac{\partial u'}{\partial\theta'}\right) + \frac{(h')^{1/2}}{r'^2}\frac{\partial^2 u}{\partial\theta'^2} - \frac{(h')^{1/2}}{r'^2(1-\theta')}\frac{\partial u}{\partial\theta'}\right] \quad (6)$$

$$\rho' u'\frac{\partial h'}{\partial r'} + \rho'\frac{v}{r'}\frac{\partial h'}{\partial\theta'} = \frac{u(\gamma-1)}{\gamma}\frac{\partial p'}{\partial r'} + \frac{1}{R_e P_r\theta_m}\left[\frac{1}{2(h')^{1/2}}\left(\frac{1}{r'}\frac{\partial h'}{\partial\theta'}\right)^2 + \frac{(h')^{1/2}}{r'^2}\frac{\partial^2 h'}{\partial\theta'^2} - \frac{(h')^{1/2}}{r'^2(1-\theta')}\frac{\partial h'}{\partial\theta'}\right] + \frac{(h')^{1/2}}{4R_e\theta_m}\left(\frac{1}{r'}\frac{\partial u}{\partial\theta}\right)^2 \quad (7)$$

where $R_e = \rho_0 h_0 r^*\theta_m/2\mu_0$.

Crank-Nicolson differences were chosen for approximating the partial derivatives in Eqs. (6) and (7) because of their superiority with respect to stability and convergence.[8,9] The difference grid is shown in Fig. 1. Substitution of the finite-difference approximations into Eqs. (6) and (7) gives equations of the form

$$A_n U_{m+1,n-1} + B_n U_{m+1,n} + C_n U_{m+1,n+1} + D_n h'_{m+1,n-1} + E_n h'_{m+1,n} + F_n h'_{m+1,n+1} = G_n \quad (8)$$

These equations give $2N - 4$ equations in $2N$ unknowns since from symmetry only half of the flowfield need be considered. The other four equations were determined from the

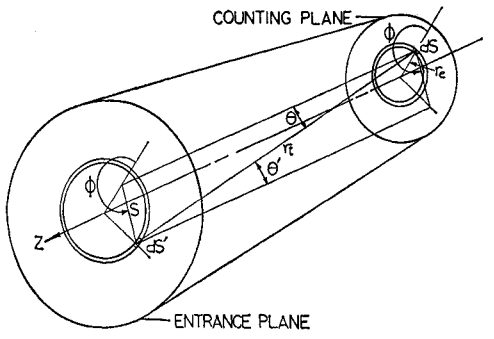

Fig. 2 Diffusion flow geometry.

boundary conditions. The boundary conditions at the centerline are given as

$$\frac{1}{r'}\frac{\partial u'}{\partial \theta'}\bigg|_{\theta'=1} = 0 \quad \text{and} \quad \frac{1}{r'}\frac{\partial h'}{\partial \theta'}\bigg|_{\theta'=1} = 0 \tag{9}$$

The form of the slip velocity for flow over a flat plate is $u_s = \lambda(\partial u/\partial y)_{y=0}$, where y is the distance normal to the plate and the momentum accomodation coefficient has been assumed to be unity, a good assumption for unpolished metals.[10] This model has given good results for slightly rarefied flow.[11] Weber[1] has modified it and obtained good results for the entire flow regime in a tube. He examined the results of research by Stokes for slowly moving spheres and developed an equation for curved surfaces. Moreover, not all of the molecules at a given instant are experiencing the viscous effects of the flow; i.e., molecules emitted from the wall are not absorbed into the viscous stream until they have traveled an average of one mean free path. To account for this effect a correction factor,[1,12] the ratio of the number of molecular collisions with the wall to the molecule-molecule collisions plus the molecule-wall collisions, is applied. The resulting equation for the slip velocity is

$$u_s = K_n' \frac{1}{r'}\frac{\partial u'}{\partial \theta'}\bigg|_{\theta'=0} \tag{10}$$

where $K_n' = K_n(1 + \frac{1}{2}e^{-2r'/K_n})/(1 + \frac{1}{2}K_n/r')$.

The wall boundary condition for enthalpy must satisfy the assumption of adiabatic flow. An energy balance on a differential volume in the flow yields

$$\frac{\partial}{\partial r}(\rho v_r h_t) + \frac{1}{r}\frac{\partial}{\partial \theta}(\rho v_\theta h_t) = \frac{1}{r}\frac{\partial}{\partial \theta}(-q_\theta + \tau v_r) \tag{11}$$

Integrating over the nozzle half section and substituting Fourier's law of heat conduction and Newton's law of viscosity gives

$$\left(\frac{k}{r}\frac{\partial T}{\partial \theta} + v_r\frac{\mu}{r}\frac{\partial v_r}{\partial \theta}\right)\bigg|_{\theta=\theta_m} = 0 \tag{12}$$

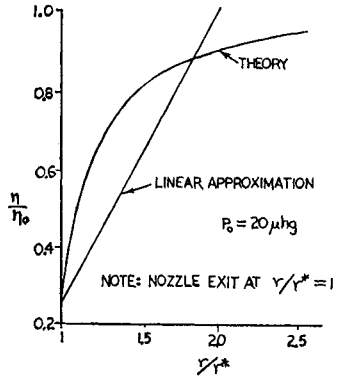

Fig. 3 Typical density distribution

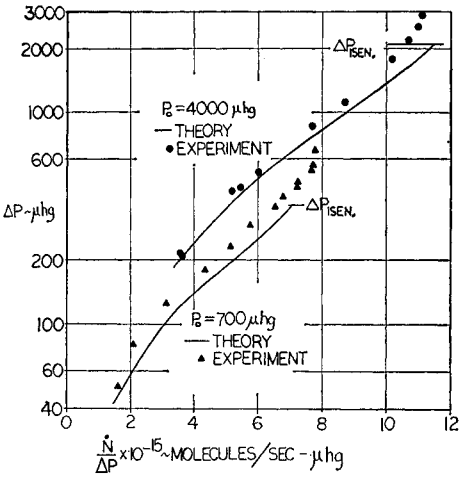

Fig. 4 Theory and experiment in the near-continuum and transition regimes.

Substituting Eq. (10) and the nondimensional variables, Eq. (12) becomes

$$\frac{1}{r'}\frac{\partial h'}{\partial \theta'}\bigg|_{\theta=0} = -\frac{P_r}{4K_n'}u_s^2 \tag{13}$$

Eqs. (13, 10, and 9), when put in finite-difference form, complete our set of $2N$ equations in $2N$ unknowns expressing v_r and h at $n + 1$ in terms of values at n.

Method of solution

The simplified N-S equations [Eq. (8)] are of tridiagonal form. They may be solved by a method first used by Flugge-Lotz and Blottner[13] and detailed for this case in Ref. 14. Then by trapezoidal integration of Eq. (5) we determine

$$P = \bar{m}\Big/\left[r'^2\int_0^1 \frac{u}{r'}(1-\theta')d\theta'\right] \tag{14}$$

where $\bar{m} = \dot{m}/r^{*2}\theta_m^2\rho_0(h_0)^{1/2}$, and ρ can then be determined from $\rho = p/R_gT$. We determine v_θ from the trapezoidal integration of Eq. (1) as

$$v_\theta = \frac{1}{\rho'(1-\theta')}\int_0^\theta \frac{(1-\theta')}{r'}\frac{\partial}{\partial r}(r'\rho' u)d\theta \tag{15}$$

All the necessary calculations may now be made for determining the variables at $m + 1$ except for $\partial p/\partial r$. Since

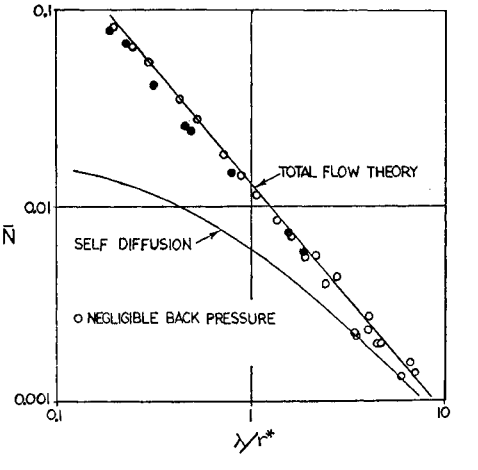

Fig. 5 Theory and experiment in the near-free-molecular regime.

$\partial p/\partial r$ is the driving force in the flow, the rest of the solution should be determined by it instead of vice versa. We evaluated it from

$$P_{m+1} = \left.\frac{\partial P}{\partial r}\right|_{m+1/2} \Delta r + P_m \tag{16}$$

and from Eq. (14) by iterating on $\partial p/\partial r$ until Eqs. (14) and (16) yielded the same value. The nozzle inlet conditions were obtained from an asymptotic solution[6] for flow in a cone far from the apex, and the solution is "Marched" downstream to the nozzle exit.

Self-Diffusion Formulation

It is necessary to determine the diffusion component which, when added to the continuum-with-slip solution, will yield the total molecular flow. The method of counting the molecules that cross a plane, which has been used successfully for constant-area flow passages,[1] is used here. It is assumed that the velocity distribution is locally Maxwellian, T is constant, and λ is constant at some mean value for any given flow conditions. Consider an elemental area in the entrance plane dS' (Fig. 2). The number of molecules which leave dS' and arrive at dS is

$$d\dot{N} = (\eta_i \bar{V}/4\pi) e^{-(r_i/\lambda)} \sin\theta \cos\theta d\theta d\phi ds \tag{17}$$

Similar expressions may be written for the flux from the nozzle wall and the flux originating from intermolecular collisions.

A linear density distribution is assumed (Fig. 3) and the integrals are formulated to obtain the diffusive flow through the exit plane in the downstream direction. The total molecular flow is then given by the difference between that in the downstream direction and that from the downstream volume, $\eta_e \bar{V} A_e/4$. The continuum solution indicated that most of the density drop in the nozzle occurs within a distance r^* of the exit plane. The effective length of the nozzle for this analysis is taken to be r^* (Fig. 3) instead of L. All lengths are subsequently nondimensionalized with respect to r^*, and the expression for the diffusive flow becomes

$$\bar{N} = \int_0^{R_0}\int_0^{\pi}\int_0^{\beta} Re'(1 - e^{-R_i/K_n}) \sin\theta \cos^2\theta d\theta d\phi dR_e' + \int_0^{R_0}\int_0^{\pi}\int_{\beta}^{\pi/2} Re' (1 - e^{R/K_n}) \sin\theta \cos^2\theta d\theta d\phi dRe' \tag{18}$$

where $R_i = r_i/r^*$, $R_e' = r_e/r^*$, and R = (distance to nozzle wall)$/r^*$, for a given θ, ϕ, and R_e' (Fig. 3). The limit β is the value of θ at which the intersection of the entrance plane and the wall occurs. The flow parameter $\bar{N}$ is given as

$$\bar{N} = \dot{N}/\lambda \bar{V} r^{*2}(dn/dz) \tag{19}$$

The integrations in Eq. (18) were performed numerically.[14]

Comparison of Theory and Experiment

Experiments were conducted on a convergent nozzle with $\theta_m = 10.33°$, $L = 1.2$ in., and exit plane radius of 0.071 in. The data obtained were $\dot{m}$, p_0, and the pressure in the chamber where the nozzle discharged, p_2. For details on the experiments, consult Refs. 14 and 15.

Fig. 3 shows both the linear density distribution assumed for the self-diffusion analysis and the true density distribution from the continuum-with-slip solution. The latter solution also indicated that the density is approximately constant in any plane normal to the nozzle axis as was assumed in the diffusion analysis.

Results for the near continuum regime are shown by the upper portion in Fig. 4. The flows represented are for $0.0025 \leq K_n \leq 0.005$. The diffusion flow component was negligible for this case, and the theoretical results represent the continuum-with-slip solution only. The correlation is good below a pressure drop of 1000 μH_g. The larger deviations at higher values may be due to the fact that p_2 was not measured in the nozzle exit. Thus, as the nozzle approaches a choking condition, the measured p_2 is less than the actual exit plane pressure p_e.

The theoretical solution indicates that the nozzle will choke at the isentropic critical pressure drop Δp_{cr}. When $\dot{m} > \dot{m}_{cr}$ appears in the theoretical solution, $\partial p/\partial r$ in the vicinity of the nozzle exit becomes infinite and no pressure can be found to satisfy the solution in the exit plane. The $\dot{m}$ just below which this occurs is $\dot{m}_{cr}$. The nozzle may actually choke at Δp_{cr} even though the experimental data does not indicate this. Again, the fact that p_2, not p_e, is measured may account for this apparent discrepancy.

The lower case in Fig. 4, $p_0 = 700$ μHg, is well within the transition regime and has $K_n \sim 0.02$. The theoretical solution indicates this in that the slip velocity is as much as 50% of the centerline velocity at the maximum $\dot{m}$. However, the diffusion is again negligible compared to the continuum-slip flow. The maximum difference between theory and experiment is ~15%. The theoretical solution has the transition flow characteristic in that it overshoots the maximum isentropic Δp by about 60 μHg.

Fig. 5 gives the results in the near-free-molecular regime. In this regime the diffusion flow component becomes a significant portion of the total flow. It varies from less than 10% of the total flow at $K_n = 0.1$ to more than 90% at $K_n = 10$.

In closing, the theoretical results indicate that the continuum equations with slip correction may be extended well beyond the continuum limit and when combined with a self-diffusion analysis will yield good results over the entire flow regime.

References

[1] Weber, S., "Uber Due Zusammenhang Zwischen Der Laminaren Stromung Der Reineu Gase Durch Rohre Und Dem Selbstdiffusions-Koeffizienten," *Math-Fvsiske Meddleller*, Bind. 28, No. 2, 1954; translantion by R. Ash and J. B. Sykes, AERE Trans 946, U.K.A.E.A. Research Group, Harwell.

[2] Ferziger, J. H., "Flow of Rarefied Gas Through A Cylindrical Tube," *The Physics of Fluids*, Vol. 10, No. 7, 1966, p. 40.

[3] Sparrow, E. M. and Johnson, V. K., "Free-Molecule Flow and Convection-Radiative Energy Transport In a Tapered Tube or Conical Nozzle," *AIAA Journal*, Vol. 1, No. 5, May 1963, pp. 1081–1087.

[4] Milligan, M. W., "Low Density Flow Through A Cylindrical Tube," Ph.D. dissertation, 1963, Univ. of Tennessee, Knoxville, Tenn.

[5] Williams, J. C., "Conical Nozzle Flow with Velocity Slip and Temperature Jump," *AIAA Journal*, Vol. 5, No. 12, Dec. 1967, pp. 2128–2134.

[6] Rae, W. J., "Some Numerical Results on Viscous Low-Density Nozzle Flows in the Slender-Channel Approximation," to be published in *AIAA Journal*.

[7] Williams, J. C., "A Study of Compressible and Incompressible Flow in Slender Channels," University of Southern California, Rept. 83-213, 1962, Univ. of Southern California.

[8] Richtmyer, G. E. and Nasow, W. R., *Finite Difference Methods for Partial Differential Equations*, 1st ed., Wiley, New York, 1960.

[9] Smith, G. D., *Numerical Solution of Partial Differential Equations*, 1st ed., Oxford University Press, New York, 1965.

[10] Hurlbut, F. C., "Studies of Molecular Scattering at the Solid Surface," *Journal of Applied Physics*, Vol. 28, No. 8, 1957, p. 844.

[11] Vincenti, W. G. and Kruger, C. H., *Introduction to Physical Gas Dynamics*, Wiley, New York, 1965.

[12] Fryer, G. M., "A Theory of Gas Flow Through Capillary Tubes," *Proceedings of the Royal Society*, Vol. A. 293, 1966, p. 329.

[13] Flugge-Lotz, I. and Blottner, F., "Computation of the Compressible Boundary-Layer Flow Including Displacement-Thickness Interaction Using Finite-Difference Methods," TR 131, 1962, Stanford Univ., Calif.

[14] Patterson, G. T., "Low Density Flow in Nozzles," Ph.D. dissertation, 1970, Univ. of Tennessee, Knoxville, Tenn.

[15] Wilkerson, H. J., "Rarefied-Gas Viscoseals," AE-70-023-8, Aug. 1970, Univ. of Tennessee, Knoxville, Tenn.